Scaling laws for natural convection boundary layer of a Pr$>$ 1 fluid on a vertical solid surface subject to a sinusoidal heating flux in a linearly-stratified ambient

Wenxian Lin[a,†], S. W. Armfield[b] and Mehdi Khatamifar[a]

[a] College of Science and Engineering, James Cook University, Townsville, QLD 4811, Australia

[b] School of Aerospace, Mechanical and Mechatronic Engineering, The University of Sydney, NSW 2006, Australia

[†] For all correspondences: wenxian.lin@jcu.edu.au

December 11, 2021

Abstract

The understanding of the transient behavior of natural convection boundary layer on a heated vertical solid surface is crucial for numerous applications. In this study, scaling analysis is performed to derive the scaling laws for the major parameters that characterize the transient behavior of natural convection boundary layer of a Prandtl number larger than 1 fluid on a vertical solid surface subject to a sinusoidal heating flux in a linearly-stratified ambient. It is found that the developed scaling laws are in good agreement with the direct numerical simulation results over wide ranges of Prandtl number, stratification parameter, and frequency of the sinusoidal heat flux.

Key words: Natural convection boundary layer; scaling; stratification; time-dependent heat flux

1 Introduction

The natural convection boundary-layer (abbreviated as 'NCBL' hereafter) flow on a heated vertical solid surface is the main mechanism for numerous practical applications, particularly in solar thermal technologies where many products and applications operate with this mechanism [1]. For example, it is this mechanism which drives air in the channels, like the Trombe wall in a solar house [2], the air flow channel in a solar air collector [3], the glazing and the absorbing wall in a solar chimney [4, 5], etc., to be heated by the absorbed solar radiation for heating and ventilation purposes. Because of this practical application importance and its fundamental significance, this topic has been extensively explored (see, e.g. [6]). Nevertheless, the research has been mostly on the scenarios where the applied temperature or heat flux on the vertical solid surface is uniformly constant or spatially altered but without temporal variation [7–15].

In practical applications, particularly in solar thermal technologies, the heating is time-varying as the solar radiation on surfaces is nearly sinusoidal [1]. Nevertheless, presently there have been very limited investigations on the unsteady NCBL flow on a vertical solid surface heated by a heat flux or temperature which changes with time [11, 16–18].

We obtained, through a thorough scaling analysis, the scalings for the key variables which characterize the behavior of unsteady NCBL flow of a homogenous $\mathrm{Pr} > 1$ fluid on a vertical solid surface subject to sinusoidal heat flux [11]. These variables include the wall temperature, the temperature boundary-layer (abbreviated as 'TBL' hereafter) thickness, the velocity boundary-layer (abbreviated as 'VBL' hereafter) thickness, the maximum vertical velocity within the VBL, the Nusselt number, and the corresponding time scales typifying the various flow development stages. These scaling predict quantitatively the associated variations of the variables with the changes of the control parameters of NCBL flow, which include the Rayleigh number (Ra), Prandtl number (Pr), frequency of the time-varying heating flux or temperature, and stratification parameter of the ambient fluid. They were validated by numerical results obtained over large ranges of the control parameters. Scaling analysis has been shown to be a very efficacious and convenient analytical approach to develop scalings for the variables describing the unsteady NCBL behavior [19]. It has been extensively used to develop scalings for various NCBL flows with different configurations and under widely varied conditions (see, *i.e.*, [11, 14, 20], for

a summary of some studies). Its ever-growing popularity in NCBL flow studies has been well evidenced by some recent studies (*e.g.*, [13, 14, 21–27]).

We extended our study [11] to the case under the time-dependent sinusoidal temperature heating condition [16] by conducting a similar scaling analysis to develop the corresponding scalings, which were also well verified by numerical results. In the past several years, we had continued the studies using similar scaling analysis and numerical simulations to derive various scaling laws for the unsteady NCBL flow under the sinusoidal heat flux or temperature for Pr $>$ 1 fluid and Pr $<$1 fluid in both homogeneous and stratified ambient fluids [28–30]. There are also some other recent studies on the unsteady NCBL flow behavior subject to different time-dependent sinusoidal temperature or heat flux for Newtonian and non-Newtonian fluids, such as [31–35]. Zhao *et al.* studied the convective instability of NCBL flow during its transition to the turbulent regime by introducing time-dependent sinusoidal temperature perturbations [17].

In the present study, the studies of [11, 16, 28, 30, 36] are extended to the unsteady NCBL flow of a Pr$>$ 1 fluid on a vertical solid surface subject to a sinusoidal heating flux in a linearly-stratified ambient. The significance to investigate the Pr$>$ 1 fluids for the scenario considered in this study is due to their numerous occurrences in nature and in practical applications. The most notable example is on the water thermal storage Trombe wall in a solar house where the absorbed sinusoidal solar radiation heats the water, which is of Pr $\sim$ 7.5 serving as a thermal storage medium, to form an unsteady NCBL flow [2, 37–39]. Another example is the unsteady NCBL flow of fresh or sea water (7.2 $\lesssim$ Pr $\lesssim$ 13.4) on the sidearm of a reservoir or ocean which is also caused by the absorbed sinusoidal solar radiation [40, 41]. Much higher Pr fluids have also be studied for many practical applications involving unsteady NCBL flows, such as engine oil nanofluids (10 $\lesssim$ Pr $\lesssim$ 1000) [42] and glycerin and its mixtures with water (50 $\lesssim$ Pr $\lesssim$ 10000) [43–45].

2 Scaling analysis

In the present study we consider the physical scenario when the right-hand side of a semi-infinite, thickness vertical solid surface is in a Newtonian ambient fluid with Pr $>$ 1 which is linearly-stratified, while its left-hand side surface is heated fully and uniformly

by a sinusoidal heat flux. It is assumed that the unsteady NCBL flow formed along the right-hand side of the solid surface is laminar and two-dimensional. The stratified ambient fluid is initially stationary and at the constant temperature gradient $\overline{T}_Y = d\overline{T}/dY^*$ in the vertical direction. The heat flux applied to the solid surface, which changes sinusoidally with time, is represented by $T_X^0(t) = -\phi_{wm}\sin(2\pi ft)$. It is assumed that both ϕ_{wm} and f are fixed at a respective value for a particular sinusoidal heat flux scenario considered. The solid surface is located at $X^* = 0$. The origin is at $Y^* = 0$, and X^* and Y^* are positive in the right and upward directions, respectively.

The governing equations for the unsteady NCBL flow are as follow, with the Boussinesq approximation for buoyancy in the Y^* momentum equation,

$$\frac{\partial u^*}{\partial X^*} + \frac{\partial v^*}{\partial Y^*} = 0, \tag{1}$$

$$\frac{\partial u^*}{\partial t} + u^*\frac{\partial u^*}{\partial X^*} + v^*\frac{\partial u^*}{\partial Y^*} = -\frac{1}{\rho}\frac{\partial P^*}{\partial X^*} + \nu\left(\frac{\partial^2 u^*}{\partial X^{*2}} + \frac{\partial^2 u^*}{\partial Y^{*2}}\right), \tag{2}$$

$$\frac{\partial v^*}{\partial t} + u^*\frac{\partial v^*}{\partial X^*} + v^*\frac{\partial v^*}{\partial Y^*} = -\frac{1}{\rho}\frac{\partial P^*}{\partial Y^*} + \nu\left(\frac{\partial^2 v^*}{\partial X^{*2}} + \frac{\partial^2 v^*}{\partial Y^{*2}}\right) + g\beta T, \tag{3}$$

$$\frac{\partial T}{\partial t} + u^*\frac{\partial T}{\partial X^*} + v^*\frac{\partial T}{\partial Y^*} + v^*\overline{T}_Y = \alpha\left(\frac{\partial^2 T}{\partial X^{*2}} + \frac{\partial^2 T}{\partial Y^{*2}}\right). \tag{4}$$

For the unsteady NCBL flow considered, the control parameters are Pr, s, and f_n, as defined below

$$\mathrm{Pr} = \frac{\nu}{\alpha}, \quad s = \frac{\overline{T}_Y}{\overline{\phi}_w}, \quad f_n = \frac{f}{V_c/L_c} = \frac{0.5/t_{ht}}{V_c/L_c} = \frac{0.5}{\tau_{ht}}, \tag{5}$$

where $\overline{\phi}_w$ is calculated by

$$\overline{\phi}_w = \frac{1}{t_{ht}}\int_0^{t_{ht}} \phi_{wm}\sin(2\pi ft)dt = \frac{2}{\pi}\phi_{wm}. \tag{6}$$

In accordance with the clear sky solar radiation model [1], only the heating part is considered in this paper, thus $2\pi f t_{ht} = \pi$, so $f = 0.5/t_{ht}$ which leads to $f_n = 0.5/\tau_{ht}$. Nevertheless, the scaling laws developed in the present study are widely applicable for many other situations in addition to the unsteady NCBL cases caused by the sinusoidal solar radiation.

Figure 1 depicts the direct numerical simulation (DNS) results of the typical development of δ_T with time at height $y = 70$ for the case of $s = 1$, $\mathrm{Pr} = 10$ and $f_n = 0.025$ (DNS run 2, as be described in the next section), where δ_T is the non-dimensional TBL thickness non-dimensionalized by L_c. In the DNS, δ_T is defined as the distance between the

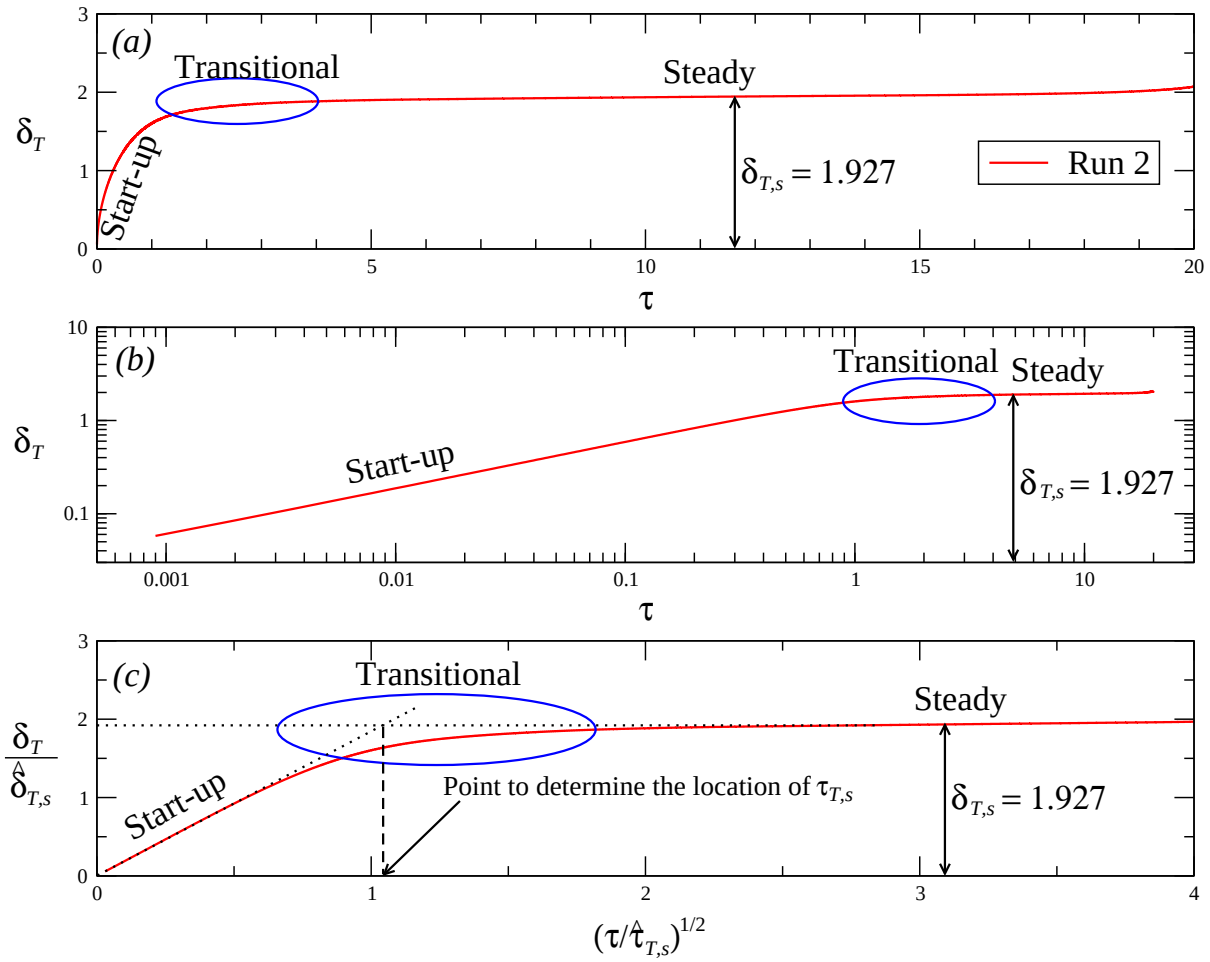

Figure 1: Time series of δ_T at $y = 70$ in Run 2: (a) in linear-linear plot and (b) in log-log plot, and (c) δ_T scaled by $\hat{\delta}_{T,s}$ and τ scaled by $\hat{\tau}_{T,s}$, where $\hat{\delta}_{T,s}$ and $\hat{\tau}_{T,s}$ are the scalings for $\delta_{T,s}$ and $\tau_{T,s}$, respectively.

right-hand side of the solid surface and the position where the temperature at y becomes to be 5% of the solid surface temperature at this y value. This figure shows that the boundary layer (abbreviated as 'BL' hereafter) undergoes three distinctive development stages; a start-up stage (abbreviated as 'SUS' hereafter) during which δ_T increases very quickly, followed by a transitional stage where the increase of δ_T is at a rate which is very small and continually reduces until zero, and thereafter, a quasi steady stage (abbreviated as 'QSS' hereafter) where δ_T is essentially constant ($\delta_T = 1.927$ for Run 2 considered). When Pr, s and f_n vary, the durations of these stage change notably, as will be described in Section 3. For the current DNS run considered, the duration of the SUS is very short (about dimensionless time duration of 1, where time is non-dimensionalized by L_c/V_c), the transitional stage is relatively long (from about 1 to 4), and the QSS is very long (from about 4 to the end of the heating cycle (20)).

For the cases considered in this paper, there are four major parameters to characterize the BL behavior, *i.e.*, the TBL thickness (Δ_T, which is the dimensional form of δ_T), inner VBL thickness (Δ_{vi}), maximum vertical velocity within the VBL (V_m^*) which occurs at $X^* = \Delta_{vi}$, and the solid surface temperature (T_w). The scaling laws for these characteristic parameters at the SUP and QSS will be obtained in the subsequent scaling analysis whereas the scaling laws at the transitional stage cannot be developed.

We follow the same procedure as taken by us in the past studies on the unsteady NCBL flows with different heating conditions and configurations, in particular that in [11, 16, 28, 29, 36]. Some details in the following scaling analysis are therefore not repeated as they can be found in these past studies.

For the unsteady NCBL flow of a Pr > 1 fluid with a background stratification on a vertical solid surface subjected to a constant heat flux ϕ_w, Armfield, Patterson & Lin [36] conducted a scaling analysis to provide the scaling laws for Δ_T, T_w and V_m^* at the SUS as follows,

$$\Delta_T \sim \alpha^{1/2} t^{1/2}, \tag{7}$$

$$T_w \sim T_X^0 \Delta_T \sim \phi_w \alpha^{1/2} t^{1/2}, \tag{8}$$

$$V_m^* \sim \frac{g\beta\phi_w \nu^{1/2} t^{3/2}}{\mathrm{Pr}^{3/2}}. \tag{9}$$

The scaling for Δ_T is also applicable for Δ_{vi} at the SUS, *i.e.*,

$$\Delta_{vi} \sim \alpha^{1/2} t^{1/2}. \tag{10}$$

For the present situation considered, *i.e.*, when the sinusoidal time-varying flux is evenly imposed on the solid surface, the scaling laws for Δ_T and Δ_{vi} at the SUS will be the same as that in the constant heat flux situation, *i.e.*, their scalings are still Eq. (7) and Eq. (10), respectively; however, the scalings for T_w and V_m^* must be revised as follows to account for the sinusoidal flux by replacing ϕ_w in their scaling laws Eq. (8) and Eq. (9) with $\phi_w(t) = \phi_{wm}\sin(2\pi ft) \sim \overline{\phi}_w\sin(2\pi ft)$,

$$T_w \sim \overline{\phi}_w\sin(2\pi ft)\alpha^{1/2}t^{1/2}, \tag{11}$$

$$V_m^* \sim \frac{g\beta\overline{\phi}_w\sin(2\pi ft)\nu^{1/2}t^{3/2}}{\mathrm{Pr}^{3/2}}. \tag{12}$$

At the time scale t_s, the SUS of the BL development terminates and the QSS commences. When the imposed flux is fixed, Armfield *et al.* [36] developed the following scaling for t_s at the height not very close to $Y^* = 0$,

$$t_s \sim \left(\frac{\mathrm{Pr}}{g\beta s\overline{\phi}_w}\right)^{1/2}. \tag{13}$$

At this time, from Eqs. (7)-(10), the corresponding scalings for Δ_T, T_w, V_m^*, and Δ_{vi} are as follows,

$$\Delta_{T,s} \sim \alpha^{1/2}t_s^{1/2} \sim \left(\frac{\alpha\nu}{g\beta s\overline{\phi}_w}\right)^{1/4}, \tag{14}$$

$$T_{w,s} \sim T_X^0\Delta_{T,s} \sim \phi_w\left(\frac{\alpha\nu}{g\beta s\overline{\phi}_w}\right)^{1/4}, \tag{15}$$

$$V_{m,s}^* \sim \frac{g\beta\phi_w\nu^{1/2}t_s^{3/2}}{\mathrm{Pr}^{3/2}} \sim \phi_w\left(\frac{g\beta}{\nu}\right)^{1/4}\left(\frac{\alpha}{s\overline{\phi}_w}\right)^{3/4}, \tag{16}$$

$$\Delta_{vi,s} \sim \alpha^{1/2}t_s^{1/2} \sim \left(\frac{\alpha\nu}{g\beta s\overline{\phi}_w}\right)^{1/4}, \tag{17}$$

where $\Delta_{T,s}$, $T_{w,s}$, $V_{m,s}^*$, and $\Delta_{vi,s}$ are the scales for Δ_T, T_w, V_m^*, and $\Delta_{vi,s}$ at t_s, *i.e.*, they represent the scales for Δ_T, T_w, V_m^*, and $\Delta_{vi,s}$ at the end of the SUS as well as at the QSS.

In the present study with the sinusoidal time-varying heat flux the above scaling laws for $\Delta_{T,s}$ and $\Delta_{vi,s}$ are still Eq. (14) and Eq. (17), respectively, similar to that at the SUS; however, similarly the above scaling laws for $T_{w,s}$ and $V_{m,s}^*$ must be revised as follows by replacing ϕ_w in their scalings with $\phi_w(t) \sim \overline{\phi}_w\sin(2\pi ft)$,

$$T_{w,s} \sim \overline{\phi}_w\sin(2\pi ft)\left(\frac{\alpha\nu}{sg\beta\overline{\phi}_w}\right)^{1/4}, \tag{18}$$

$$V^*_{m,s} \sim \overline{\phi}_w \sin(2\pi f t) \left(\frac{g\beta}{\nu}\right)^{1/4} \left(\frac{\alpha}{s\overline{\phi}_w}\right)^{3/4}, \tag{19}$$

An inspection of these scaling laws informs that when for $Y^* \gg 0$, the BL development is one-dimensional and does not depend on Y. However, when Y^* is very small, the BL development will act in the same way as that when the ambient fluid is not stratified [11,36,46], which is two-dimensional and depends on Y^*, as elaborated in detail in [28,36]. However, as this paper focuses on Y^* not very close 0 (*i.e.*, the one-dimensional flow regime), the two-dimensional BL development behavior at very small Y^* values will not be elaborated further.

The obtained scaling laws, which are in dimensional forms, can be non-dimensionalized by their respective characteristic scales typifying the unsteady NCBL flow. It is appropriate, from Eq. (14) and Eq. (16), to choose

$$L_c = \left(\frac{\alpha\nu}{g\beta s\overline{\phi}_w}\right)^{1/4}, \tag{20}$$

and

$$V_c = \overline{\phi}_w \left(\frac{g\beta}{\nu}\right)^{1/4} \left(\frac{\alpha}{s\overline{\phi}_w}\right)^{3/4}, \tag{21}$$

as the characteristic length and velocity scales, and L_c/V_c and $\overline{\phi}_w L_c$ as the characteristic time and temperature scales, respectively. With L_c, V_c, L_c/V_c and $\overline{\phi}_w L_c$, the above scaling laws for the present sinusoidal heat flux scenario can be non-dimensionalized as shown below.

At the SUS, Eqs. (7)-(10) are made dimensionless as follows,

$$\delta_T = \frac{\Delta_T}{L_c} \sim s^{1/2}\tau^{1/2}, \tag{22}$$

$$\theta_w = \frac{T_w}{\overline{\phi}_w L_c} \sim \sin(2\pi f_n \tau) s^{1/2}\tau^{1/2}, \tag{23}$$

$$v_m = \frac{V^*_m}{V_c} \sim \sin(2\pi f_n \tau) s^{3/2}\tau^{3/2}, \tag{24}$$

$$\delta_{vi} = \frac{\Delta_{vi}}{L_c} \sim s^{1/2}\tau^{1/2}, \tag{25}$$

Thess dimensionless scaling laws (22)-(25) are only applicable for $\tau < \tau_s$. From Eq. (13), the scaling law for the dimensionless time scale, τ_s, is as follows,

$$\tau_s = \frac{t_s}{(L_c/V_c)} \sim \frac{1}{s}. \tag{26}$$

At the QSS (*i.e.*, at τ_s), the scaling laws (14), (18), (19), and (17) can be made dimensionless as follows,

$$\delta_{T,s} = \frac{\Delta_{T,s}}{L_c} \sim 1, \tag{27}$$

$$\theta_{w,s} = \frac{T_{w,s}}{\overline{\phi}_w L_c} \sim \sin(2\pi f_n \tau_s), \tag{28}$$

$$v_{m,s} = \frac{V^*_{m,s}}{V_c} \sim \sin(2\pi f_n \tau_s), \tag{29}$$

$$\delta_{vi,s} = \frac{\Delta_{vi,s}}{L_c} \sim 1. \tag{30}$$

3 Numerical validation of the scalings

The scaling laws obtained above are assessed and validated numerically with DNS runs. To examine the roles of Pr, s and f_n in the scaling laws, a total of 14 DNS runs were carried out, with detains of these runs presented in Table 1; five (Runs 1-5) are at varying Pr over $5 \leq \text{Pr} \leq 100$ with fixed $s = 1$ and $f_n = 0.025$ to show the Pr dependence; six (Runs 2 and 6-10) are for the variation of s in the range of $0.2 \leq s \leq 20$ at $\text{Pr} = 10$ and $f_n = 0.025$ to show the s dependence; and five (Runs 2 and 11-14) are for the variation of f_n over $0.005 \leq f_n \leq 0.1$ at fixed $s = 1$ and $\text{Pr} = 10$ to illustrate the f_n dependence. As the scaling laws are developed assuming $\text{Pr} \gg 1$, the minimum value of Pr selected is 5. It should be noted that the selected ranges of Pr, f_n and s cover a wide range of practical application scenarios. For example, for the case of the water thermal storage Trombe wall in a solar house, one of the commonly used materials for the absorbing plate, which is the vertical wall of the water storage tank where the absorbed solar radiation is transferred into the tank to heat the water through conduction and natural convection, is stainless steel which has the thermal conductivity of about 15 W/(m·K) [47]. With the thermal properties of water at 30 ^{o}C being $\rho = 996$ kg/m^3 (density), $\beta = 3 \times 10^{-4}$ 1/K (thermal expansion coefficient), $\text{Pr} = 5.4$, and $\nu = 8 \times 10^{-5}$ m^2/s [47], respectively, if it is assumed that $s = 1$ and the typical average solar radiation absorbed by the plate is 500 W/m^2 [1], which gives $\overline{\phi}_w = 33.3$ K/m, the characteristic velocity of the NCBL flow on the plate is on the order of 0.0014 m/s from Eq. (21) and for the vertical plate of the length of 1 m, the corresponding half period of the sinusoidal heat flux (the heating period of time) is on the order of 19.66 hours, 9.83 hours, 3.93 hours and 1.97 hours for $f_n = 0.005$, 0.01,

Table 1: Values of Pr, s, f_n, τ_{ht}, $\tau_{T,s}$, and $\tau_{vi,s}$ for the 14 DNS runs.

Run	s	Pr	f_n	τ_{ht}	$\tau_{T,s}$	$\tau_{vi,s}$
1	1	5	0.025	20	1.065	1.641
2	1	10	0.025	20	1.065	1.243
3	1	20	0.025	20	1.067	0.962
4	1	50	0.025	20	1.067	0.709
5	1	100	0.025	20	1.067	0.579
6	0.2	10	0.025	20	5.325	6.216
7	0.5	10	0.025	20	2.130	2.248
8	5	10	0.025	20	0.213	0.248
9	10	10	0.025	20	0.109	0.124
10	20	10	0.025	20	0.053	0.062
11	1	10	0.005	100	1.065	1.244
12	1	10	0.01	50	1.065	1.243
13	1	10	0.05	10	1.065	1.243
14	1	10	0.1	5	1.065	1.243

0.025, and 0.05, respectively, while for the plate length of 2 m, these values change to 39.32 hours, 19.66 hours, 7.86 hours, and 3.93 hours for $f_n = 0.005$, 0.01, 0.025, and 0.05, respectively, and when the plate length becomes 0.5 m, these values change to 9.83 hours, 4.91 hours, 1.97 hours, and 0.98 hours for $f_n = 0.005$, 0.01, 0.025, and 0.05, respectively. All these are applicable for practical applications. As s, heat flux and materials for the plate and the fluid can vary substantially, the range of $0.005 \leq f_n \leq 0.1$ is therefore able to cover a wide range of practical application scenarios.

All numerical simulations were conducted with our in-house code used in [11, 28, 29] and a series of our other past studies, such as [10, 36, 48]. As the numerical methodology, meshes, benchmarking of the code, etc., were detailed in those papers, particularly in [11, 28], they will not be presented here to avoid repetition.

As discussed above, the obtained scaling laws are one-dimensional and do not depend on y, if $y \gg 0$. The two-dimensional and y dependent behavior of the BL development is present only when y is very small, which is not the focus of the present study. The

DNS results show that for all runs the regions for the two-dimensional and y dependent behavior are with very small y values (less than 5). Hence only the DNS results at $y = 70$ will be used subsequently.

3.1 Validation of the scaling laws for δ_T scales

As shown in Fig. 1, the development of the TBL in terms of δ_T undergoes three distinctive stages; a SUS during which δ_T increases very quickly, followed by a transitional stage where the increase of δ_T is at a rate which is very small and continually reduces until zero, and thereafter, a QSS where δ_T is essentially constant. However, as discussed above, only the scalings at the SUS and QSS were obtained and the scaling analysis was unable to give the scaling laws at the transitional stage. In addition, the exact times for the end of the SUS and the transitional stage are not easily defined and thus determined. To quantitatively validate the obtained scaling laws at the SUS and QSS with the DNS results, it will appropriate to just assume that the BL development consists of the SUS and QSS, *i.e.*, τ_s is used as the time scale for both the end of the SUS and the commencement of the QSS. The determination of this time scale $\tau_{T,s}$ for δ_T is demonstrated in Fig. 1(c). The scaling for δ_T at the SUS is Eq. (22) while the scaling for δ_T at the QSS is Eq. (27). The scaled time series of δ_T at the SUS is a straight line as shown in the figure, when δ_T and τ are scaled by their respective scales $\hat{\delta}_{T,s} = 1$ and $\hat{\tau}_{T,s} = 1/s$ based on the scalings (27) and (26). As $\delta_T/\hat{\delta}_{T,s}$ is a constant at the QSS, an appropriate way to determine $\tau_{T,s}$ for $\delta_{T,s}$ is to find the intersection of $\delta_T/\hat{\delta}_{T,s}$ against $(\tau/\hat{\tau}_{T,s})^{1/2}$ at the SUS and QSS. For Run 2, as shown in Fig. 1(c), $\delta_T/\hat{\delta}_{T,s} = 1.867(\tau/\hat{\tau}_{T,s})^{1/2}$ at the SUS and $\delta_T/\hat{\delta}_{T,s} = 1.927$ at the QSS, which gives the intersection at $\tau_{T,s} = (1.927/1.867)^2/s = 1.065/1 = 1.065$. The values of $\tau_{T,s}$ for all other runs considered are determined in the same way, and are presented in Table 1.

The dependence of δ_T on s, Pr and f_n is also clearly shown in the development of δ_T with time as presented in Fig. 2. The results in Fig. 2(a-b) demonstrate that at the SUS, s has a strong effect on δ_T, as the growth rate of δ_T with time reduces when s is increased monotonically, but the rate of the reduction decreases gradually, meanwhile, the time to approach the QSS reduces as well, which agrees with the scaling (26). Nevertheless, $\delta_{T,s}$ essentially does not change when s varies at the QSS, *i.e.*, $\delta_{T,s} \approx 1.927$, confirming the

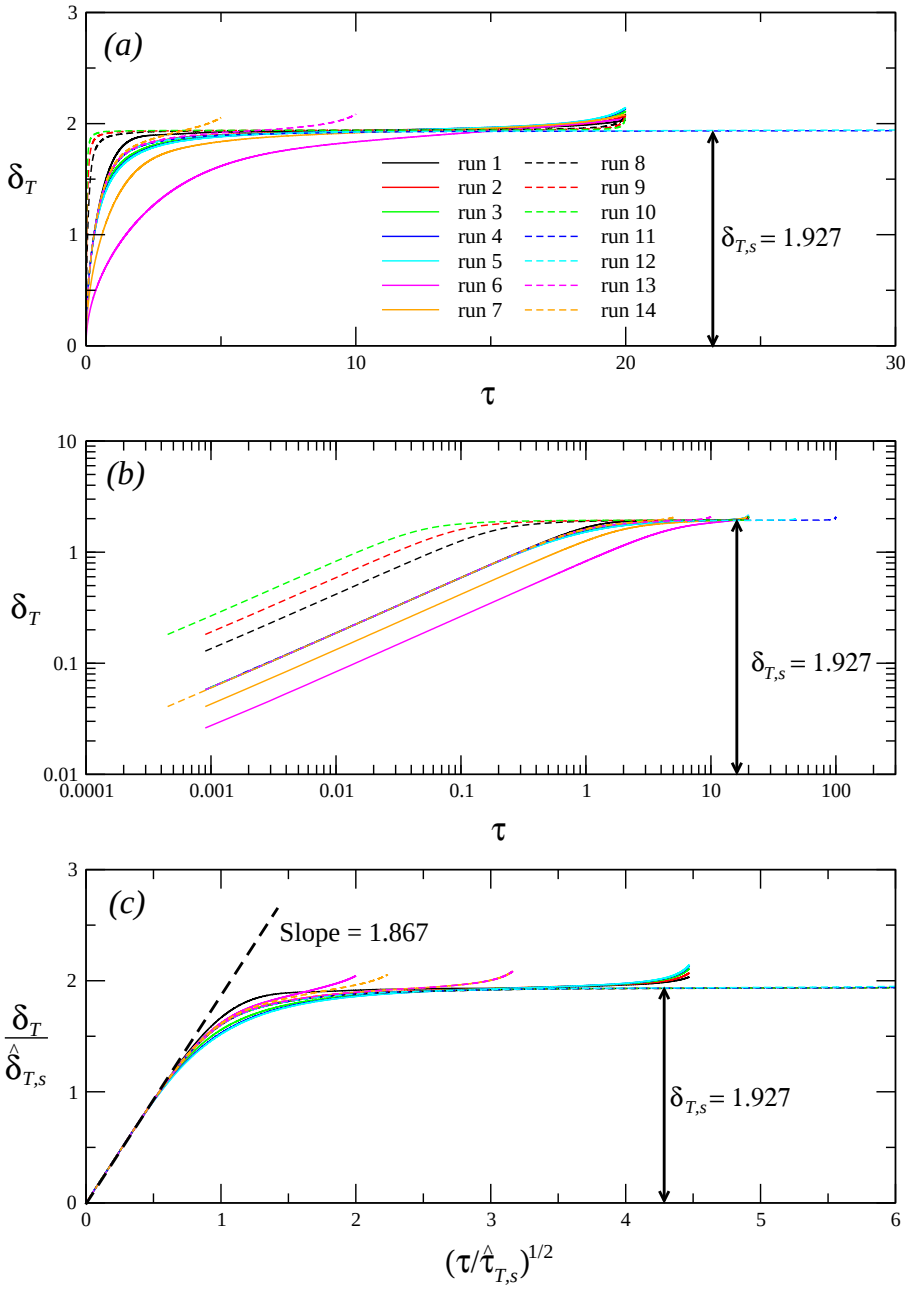

Figure 2: The raw (a in linear-linear plot and b in log-log plot) and scaled (c) time series of δ_T for all 14 runs, where $\hat{\delta}_{T,s} = 1$ and $\hat{\tau}_{T,s} = 1/s$ are the scalings for $\delta_{T,s}$ and $\tau_{T,s}$, respectively.

scaling (27). The scaling laws (22), (27), and (26) show no Pr dependence. The numerical results in the figure verify this as there are only slight differences when δ_T develops over the time, which occur at the transitional stage. Likewise, the scaling laws do not depend on f_n, which is also confirmed by the results of the figure.

The scaling laws for δ_T at the SUS and $\delta_{T,s}$ at the QSS as well as $\tau_{T,s}$, *i.e.*, Eqs. (22), (27), and (26) can be quantitatively validated as well. Figure 2(c) contains the scaled time series of δ_T. The results reveal that the scaled time series overlap each other very well at the SUS and QSS, giving the following quantified scaling law for δ_T at the SUS,

$$\frac{\delta_T}{\hat{\delta}_{T,s}} = 1.867 \left(\frac{\tau}{\hat{\tau}_{T,s}} \right)^{1/2}, \tag{31}$$

which can be written as follows with $\hat{\delta}_{T,s} = 1$ and $\hat{\tau}_{T,s} = 1/s$,

$$\delta_T = 1.867 s^{1/2} \tau^{1/2}. \tag{32}$$

This validates quantitatively the scaling law (22) for δ_T at the SUS. As presented in Table 1, for all DNS runs with different Pr and f_n values but the fixed $s = 1$, the values of $\tau_{T,s}$ are essentially the same, *i.e.*, $\tau_{T,s} = 1.065$, indicating that $\tau_{T,s}$ is independent of Pr and f_n. For Runs 2 and 6-10 with varying s and the fixed Pr = 10 and $f_n = 0.025$, the values of $\tau_{T,s}$ are 5.325*0.2=1.065, 2.130*0.5=1.065, 0.213*5=1.065, 0.109*10=1.090, and 0.053*20=1.060 for s = 0.2, 0.5, 5, 10, and 20, respectively. These values are either at the same value (1.065) as that for other runs or just marginally different, which validate quantitatively the scaling (26). The results presented in Fig. 2((c)) further show this, which give the following quantified scaling for $\tau_{T,s}$,

$$\tau_{T,s} = \frac{1.065}{s}. \tag{33}$$

The scaling laws for θ_w, v_m and δ_{vi} can be validated in the same way as that for θ_w, as detailed below.

3.2 Validation of the scaling laws for θ_w scales

The development θ_w with time for all 14 runs are depicted in Fig. 3 to show the dependence on s, Pr, and f_n. It is noted that they largely follow the time series of the applied heat flux. However, there are noticeable deviations at the SUS of the BL development, in the

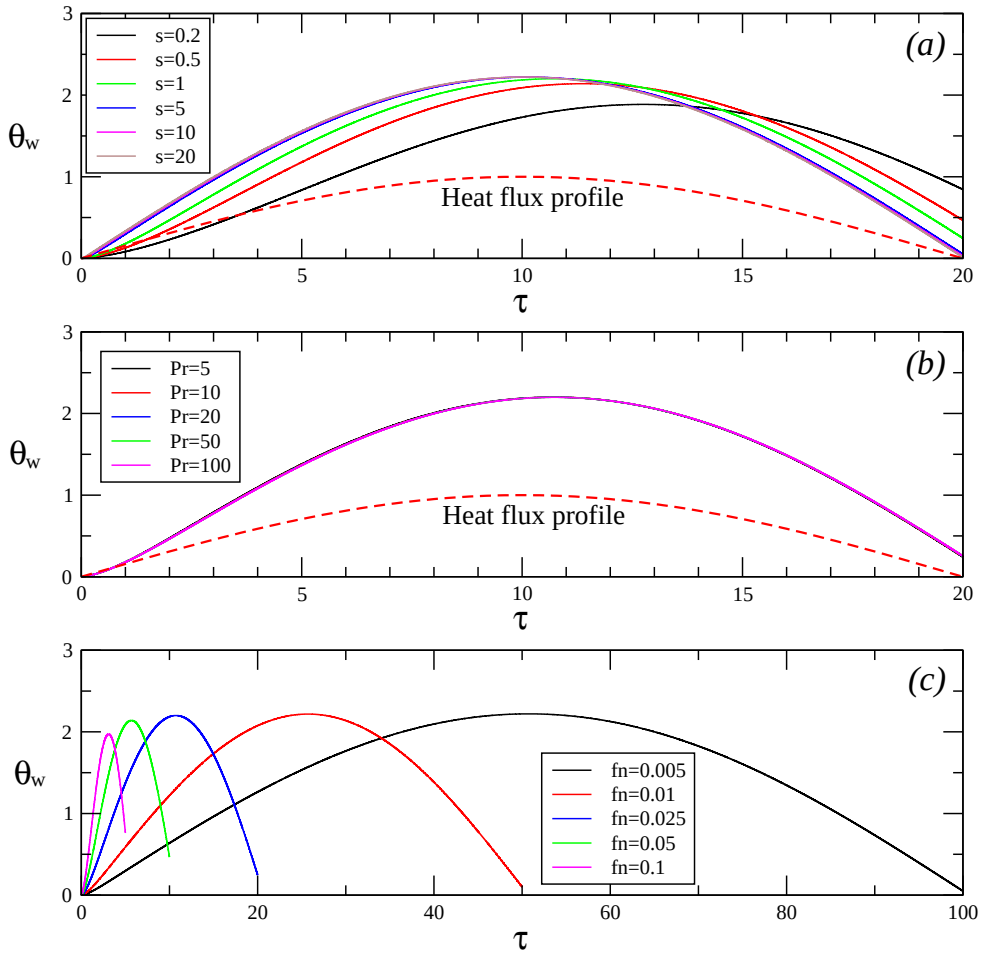

Figure 3: Time series θ_W with (a) s variation (runs 2, 6-10), all with Pr $= 10$ and $f_n = 0.025$, (b) Pr variation (runs 1-5), all with $s = 1$ and $f_n = 0.025$, and (c) f_n variation (runs 2, 11-14), all with Pr $= 10$ and $s = 1$.

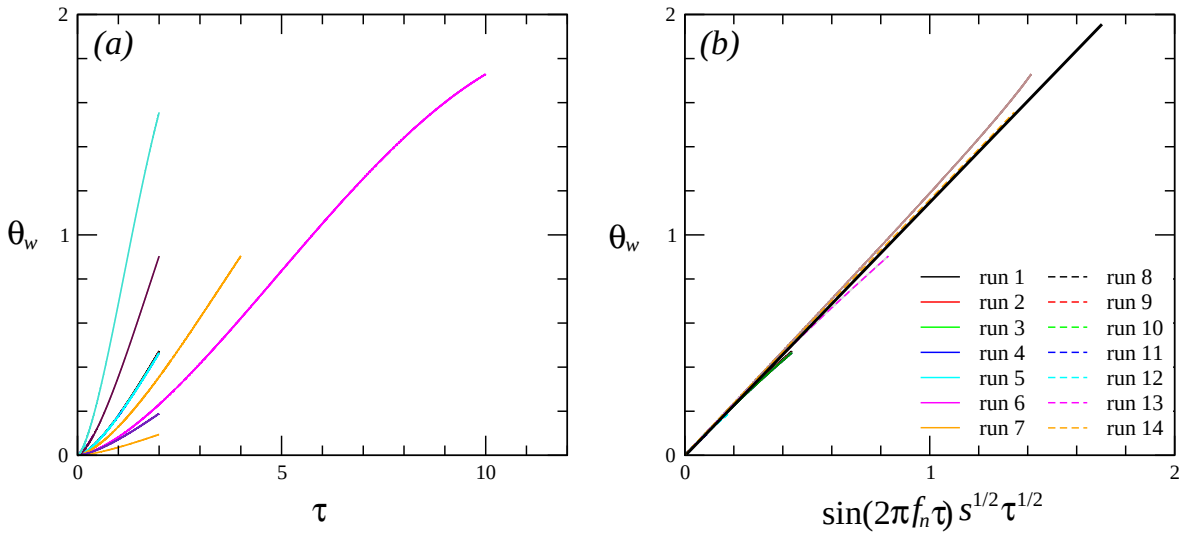

Figure 4: Time series of θ_w at the SUS: Raw (a) and scaled (b).

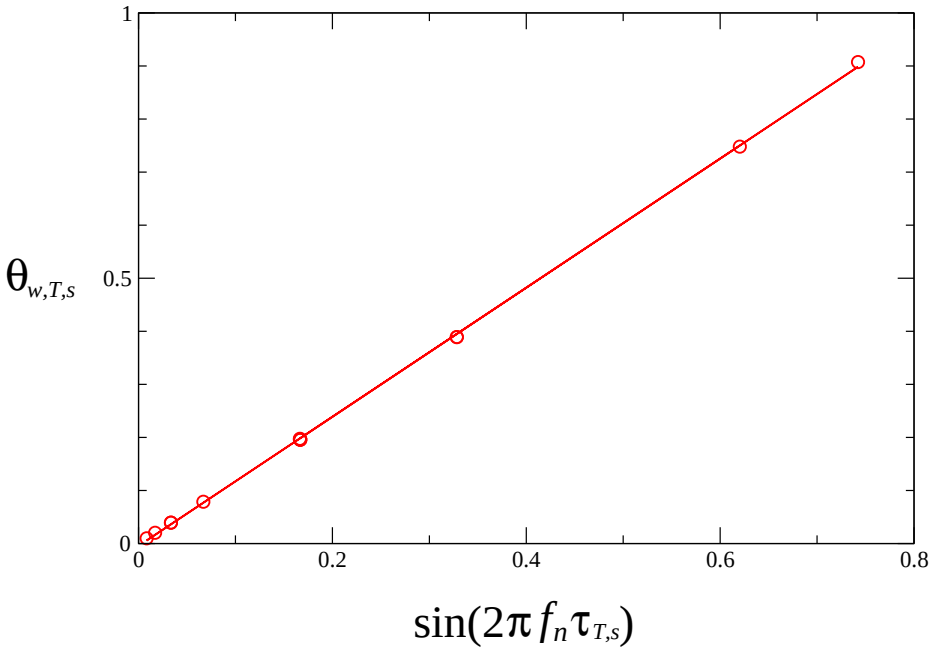

Figure 5: $\theta_{w,T,s}$ plotted against $\sin(2\pi f_n \tau) s^{1/2} \tau^{1/2}$ for all DNS runs.

profile of the time series, in the time for the peak value of θ_w, and in the value of θ_w at the end of the heating cycle, although these deviations vary significantly for different s, Pr and f_n values. One considerable difference from δ_t is that θ_w continues to increase after the SUS, and soon becomes essentially follow the heat flux profile, although with a time delay which varies when s, Pr and f_n change. It is observed that Pr does not affect the time series of θ_w, as clearly shown in Fig. 3(b), however, both s and f_n do. As shown in Fig. 3(a), when s is small ($s \leq 1$), the influence from Pr is significant; the SUS is long, as predicted by the scaling law (26); the time series at this early stage deviates noticeably from the applied heat flux profile; the time for θ_w to attain its maximum (the time delay) is large and its maximum is smaller; and θ_w at the end of the heating cycle is large. However, these deviations reduce significantly when s increases, indicating that its effect on θ_w decreases, and when $s \geq 5$, the time series of θ_w of all three large s values overlap each other and essentially follow the applied heat flux profile, except with some slight deviations still occurring at the SUSs which are very short as predicted by the scaling (26), showing that the s effect is negligible when it is very large (much largen than 1). As shown in Fig. 3(c), some of the above observations on the effect of s are also true for the effect of f_n; the development θ_w with time also largely obeys the sinusoidal heat flux profile, again with some deviations at the SUS, the time to reach the maximum and the value of the maximum, as well as the value of θ_w at the end of the heat cycle. Such deviations reduce when f_n decreases.

At the SUS, the scaling law for θ_w is (23). The numerical results in Fig. 4(b) validate this scaling law, as θ_w is found to increase linearly with $\sin(2\pi f_n \tau) s^{1/2} \tau^{1/2}$ for each run at the SUS, and more importantly, such linear relations of all runs overlap very well and collapse onto the following quantified linear relation,

$$\theta_w = 1.12 \sin(2\pi f_n \tau) s^{1/2} \tau^{1/2}. \tag{34}$$

Although it is difficult to determine the time characterizing the end of the SUS which is also the commencement time for the QSS, and the corresponding value of θ_w at this time from the time series of θ_w as presented in Fig. 3, it is still reasonable and justifiable to use $\tau_{T,s}$ to approximate this time. Figure 5 presents θ_w at this time $\tau_{T,s}$, *i.e.*, $\theta_{w,T,s}$, plotted against $\sin(2\pi f_n \tau_{T,s}) s^{1/2} \tau^{1/2}$. It is seen that the relation between $\theta_{w,T,s}$ and

$\sin(2\pi f_n \tau_{T,s}) s^{1/2} \tau^{1/2}$ is linear and can be quantified as follows,

$$\theta_{w,T,s} = 1.216 \sin(2\pi f_n \tau) s^{1/2} \tau^{1/2}, \tag{35}$$

with the linear regression coefficient of $R^2 = 0.9999$. This clearly shows that the scaling (28) for $\theta_{w,T,s}$ is valid.

3.3 Validation of the scaling laws for v_m scales

Figure 6 presents the numerically obtained results for the development of v_m with time. Compared it to Fig. 3, it is noted that the s, Pr, and f_n have very similar effects on v_m to that on θ_w, because of the same term $\sin(2\pi f_n \tau)$ for v_m at the SUS and $\sin(2\pi f_n \tau_{T,s})$ for $v_{m,T,s}$ at the end of the SUS and the beginning of the QSS, as shown in the scaling laws (24) and (29), respectively, and thus are not repeated here.

In Fig. 7(b), the scaled development v_m with time at the SUS are shown for all runs, where the time scaled by $\sin(2\pi f_n \tau) s^{3/2} \tau^{3/2}$, which is the scaling law (24) for v_m at the SUS. The results show that the relation between v_m and $\sin(2\pi f_n \tau) s^{3/2} \tau^{3/2}$ for each run at the SUS is approximately linear, which validates the scaling (24), although there are noticeable differences among runs. The results show that the majority of the runs fall approximately onto the following quantified relation,

$$v_m = 0.21 \sin(2\pi f_n \tau) s^{3/2} \tau^{3/2}. \tag{36}$$

Similar to that for θ, it is also difficult to determine the time signifying the end of the SUS and the commencement time for the QSS for v_m, and thus the corresponding value of v_m at this time from the time series of v_m as presented in Fig. 6. Again $\tau_{T,s}$ is believed to be the approximate of this time. The numerical results depicted in Fig. 8 confirms this, where v_m at $\tau_{T,s}$, *i.e.*, $v_{m,T,s}$ is plotted against $\sin(2\pi f_n \tau_{T,s})$. It is seen that the relation between $v_{m,T,s}$ and $\sin(2\pi f_n \tau_{T,s})$ is linear and can be quantified as follows,

$$v_{m,T,s} = 0.21 \sin(2\pi f_n \tau), \tag{37}$$

with the linear regression coefficient of $R^2 = 0.9988$. This clearly shows that the scaling (29) for $v_{m,T,s}$ is valid.

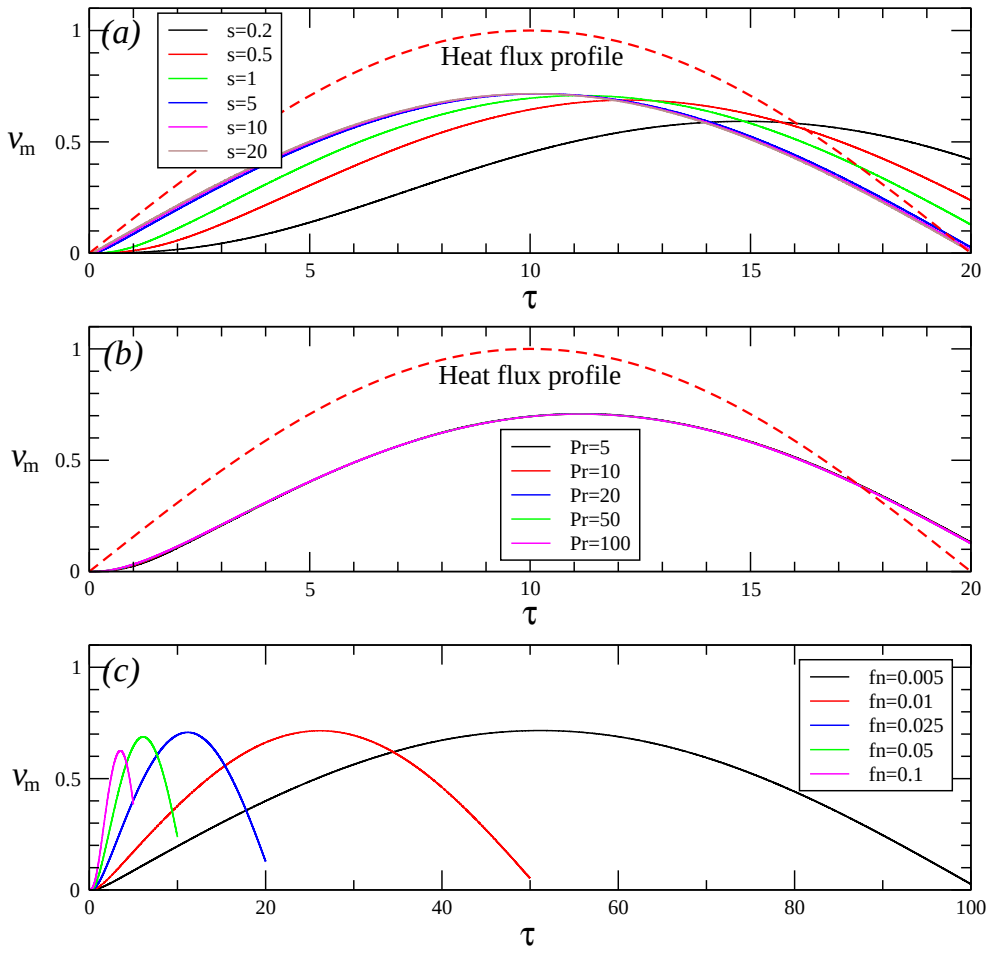

Figure 6: Time series v_m with (a) s variation (runs 2, 6-10), all with Pr $= 10$ and $f_n = 0.025$, (b) Pr variation (runs 1-5), all with $s = 1$ and $f_n = 0.025$, and (c) f_n variation (runs 2, 11-14), all with Pr $= 10$ and $s = 1$.

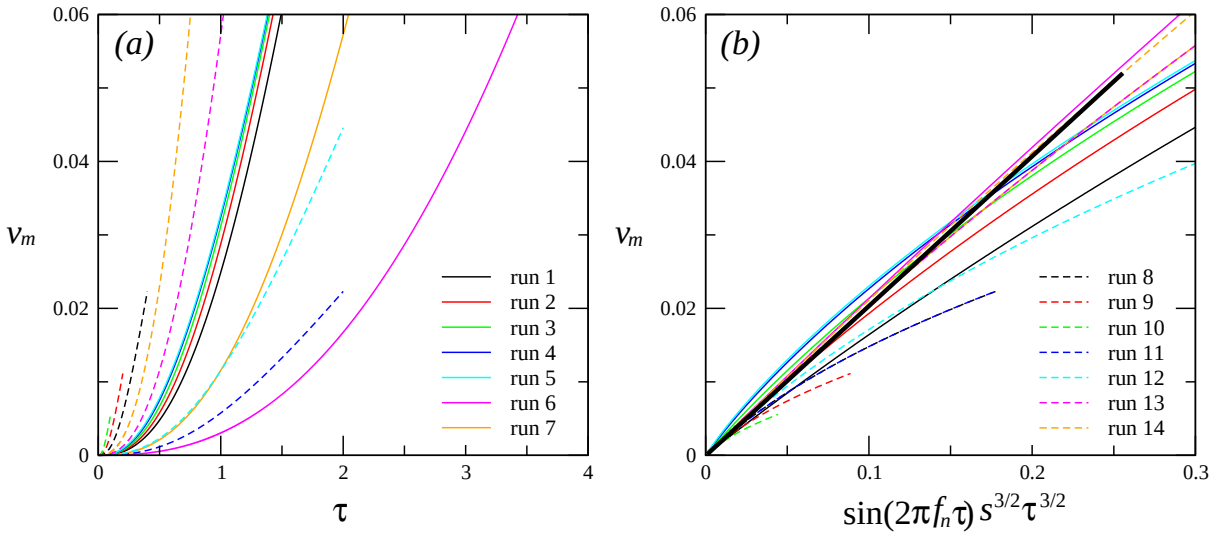

Figure 7: Time series of v_m at the SUS: Raw (a) and scaled (b).

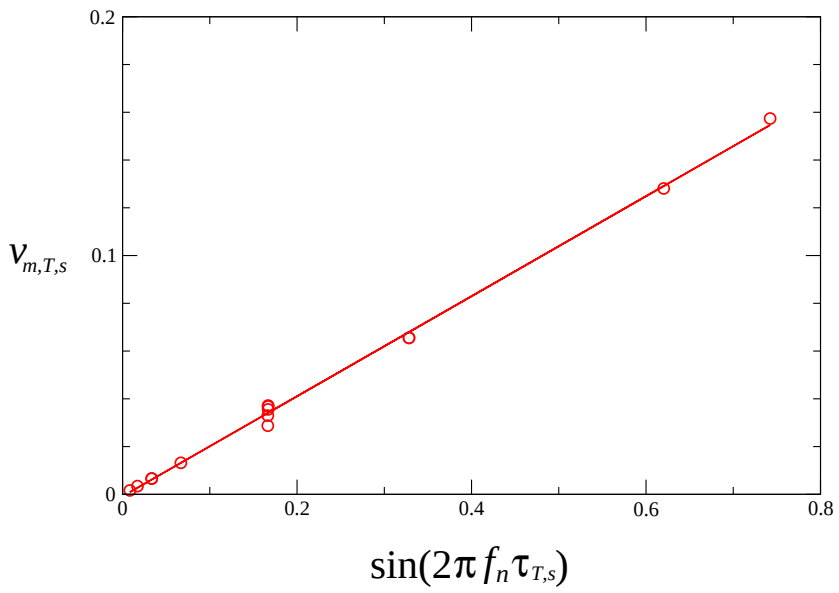

Figure 8: $v_{m,T,s}$ plotted against $\sin(2\pi f_n \tau) s^{1/2} \tau^{1/2}$ for all DNS runs.

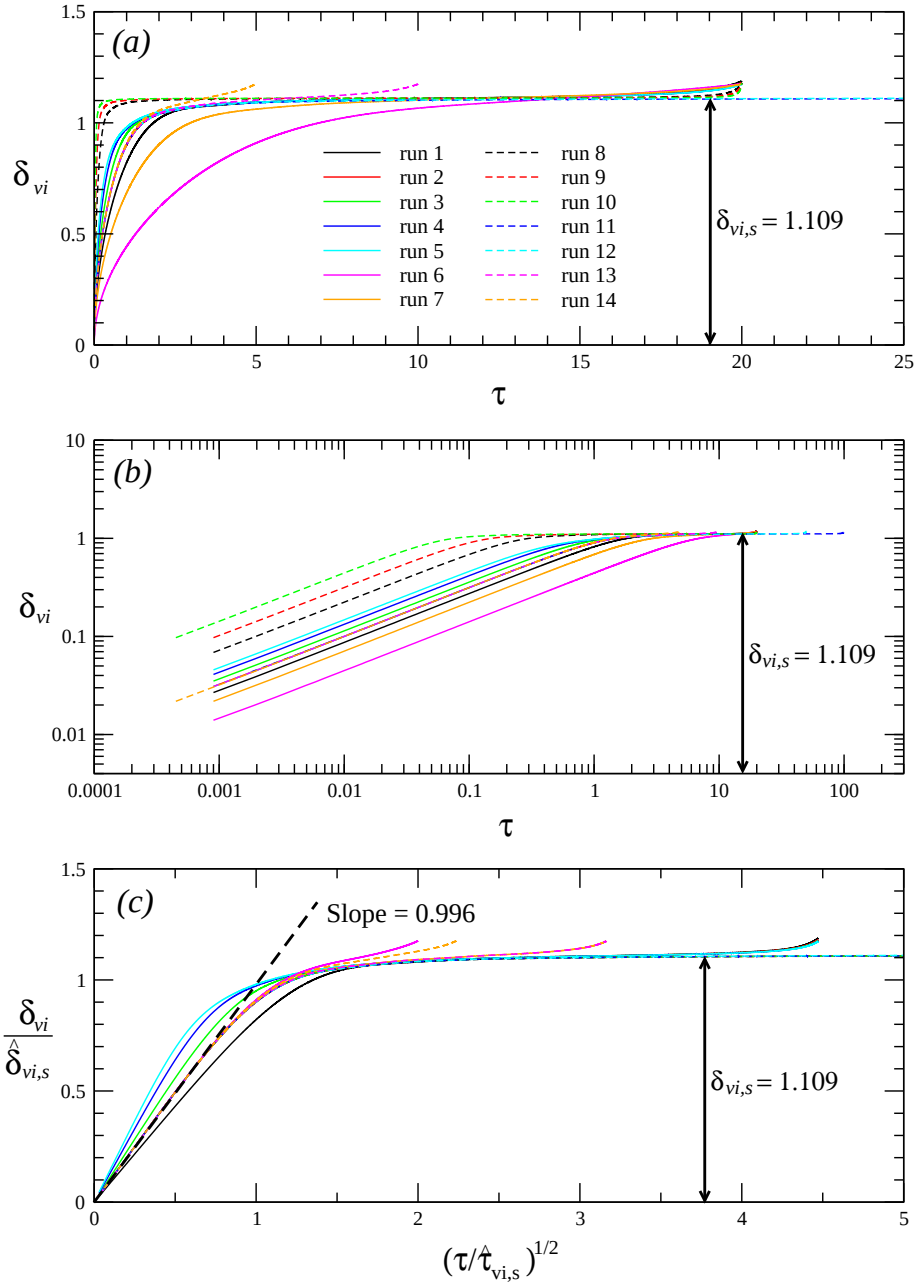

Figure 9: The raw (a in linear-linear plot and b in log-log plot) and scaled (c) time series of δ_{vi} for all 14 runs, where $\hat{\delta}_{vi,s} = 1$ and $\hat{\tau}_{T,s} = 1/s$ are the scalings for $\delta_{vi,s}$ and $\tau_{T,s}$, respectively.

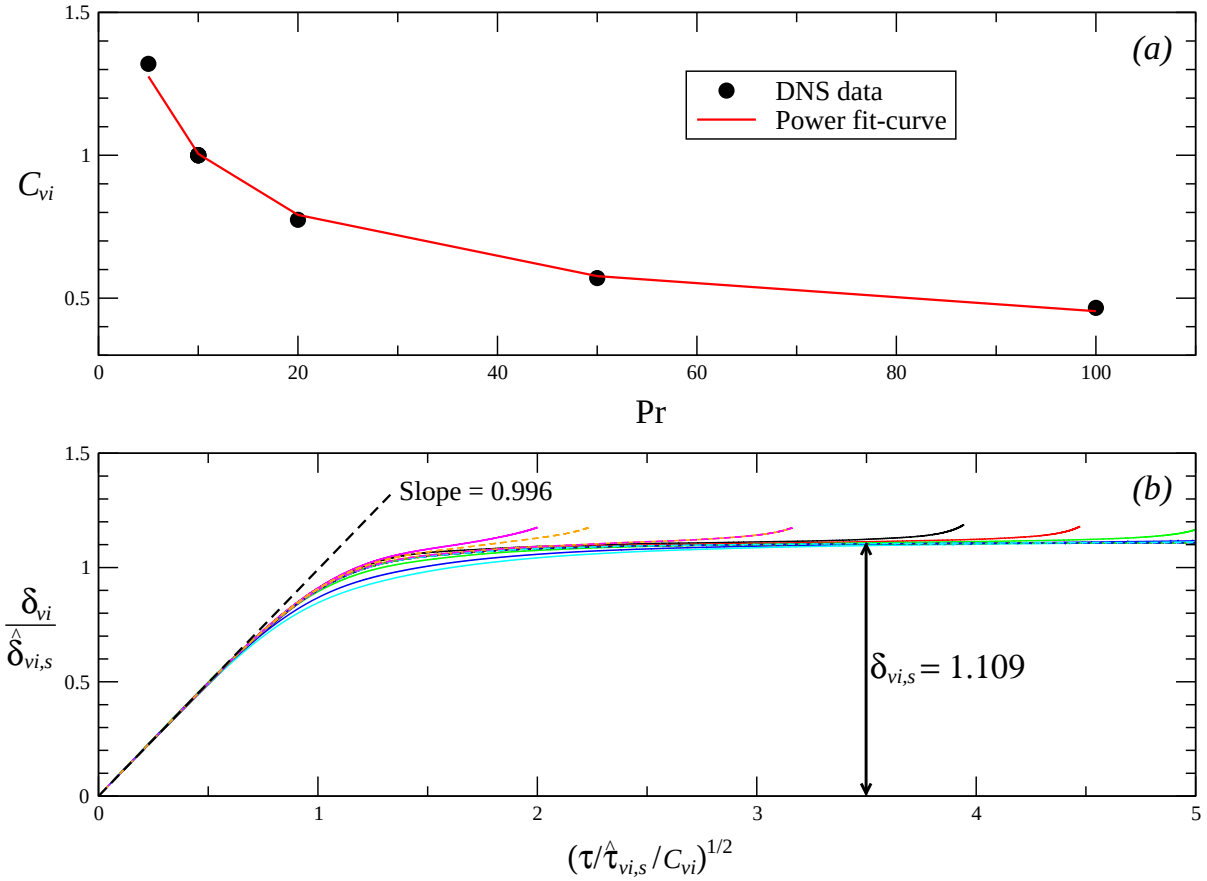

Figure 10: (a) C_{vi} plotted against Pr and (b) the scaled time series of δ_{vi} with Pr modification for all 14 runs, where $\hat{\delta}_{vi,s} = 1$ and $\hat{\tau}_{T,s} = 1/s$ are the scalings for $\delta_{vi,s}$ and $\tau_{vi,s}$, respectively.

3.4 Validation of the scaling laws for δ_{vi} scales

Figure 9 presents the raw and scaled developments of δ_{vi} with time, which clearly show the dependence of δ_{vi} on s, Pr and f_n. Figure 9(a-b) demonstrates that at the SUS, s has a strong effect on δ_{vi}, which is very similar to that on δ_T as shown in Fig. 2. The dependence of δ_{vi} on f_n is also very similar to that of δ_T. However, different from that for δ_T, Pr has an effect on δ_{vi} as the time series with varying Pr values do not overlap, but deviate noticeably from each other, although only at the SUS, as clearly shown in the figure. At the QSS, $\delta_{vi,s}$ is essentially the same for all runs, *i.e.*, $\delta_{vi,s} \approx 1.109$, confirming the scaling (30). The dependence of δ_{vi} on s and f_n, *i.e.*, the scaling (25) and (26), is verified by the DNS results in Fig. 9(c), which shows that for all Pr = 10 runs, the relation between $\delta_{vi}/\hat{\delta}_{vi,s}$ and $(\tau/\hat{\tau}_{vi,s})^{1/2}$ at the SUS is linear and can be quantified by the DNS results as follows,

$$\frac{\delta_{vi}}{\hat{\delta}_{vi,s}} = 0.996 \left(\frac{\tau}{\hat{\tau}_{vi,s}}\right)^{1/2}, \tag{38}$$

which can be written as follows with $\hat{\delta}_{vi,s} = 1$ and $\hat{\tau}_{vi,s} = 1/s$,

$$\delta_{vi} = 0.996 s^{1/2} \tau^{1/2}. \tag{39}$$

From the intersection between $\delta_{vi}/\hat{\delta}_{vi,s}$ and $(\tau/\hat{\tau}_{vi,s})^{1/2}$ at the SUS and QSS, it is also found that

$$\tau_{vi,s} = \frac{1.243}{s}, \tag{40}$$

for all runs with Pr = 10, as shown in Table 1.

However, as noted above, when Pr varies, although the relation between $\delta_{vi}/\hat{\delta}_{vi,s}$ and $(\tau/\hat{\tau}_{vi,s})^{1/2}$ at the SUS for the run is still linear, the slope differs and monotonically increases, from 0.866 at Pr = 5 to 1.457 at Pr = 100. This means that the obtained scaling (25) does not predict the Pr effect, and thus needs to be modified to account for the Pr dependence.

In Fig. 10, the value of C_{vi}, which is the ratio of the slope with Pr $\neq$ 10 and the slope with Pr = 10. The regression gives the following empirical relation for C_{vi},

$$C_{vi} = 2.224 \mathrm{Pr}^{-0.35}, \tag{41}$$

with the regression coefficient of $R^2 = 0.9971$. With the Pr dependence modification, it is found that the scaled developments of δ_{vi} with time at the SUS for all runs collapse onto

the same straight line quantified by the following relation,

$$\delta_{vi} = 0.668\mathrm{Pr}^{0.175} s^{1/2} \tau^{1/2}. \tag{42}$$

4 Conclusions

A set of scaling laws have been developed to delineate the intrinsic behavior of unsteady NCBL flow of a linearly-stratified Pr $>$ 1 fluid on a semi-infinite vertical solid surface subject to a sinusoidal heat flux. There scalings are represented in terms Pr, s and f_n, which are the major parameters controlling the flow.

The obtained scaling laws are validated and quantified with DNS runs over $0.2 \leq s \leq 20$, $5 \leq \mathrm{Pr} \leq 100$, and $0.005 \leq f_n \leq 0.1$. It is found that the numerical results are in general in good agreement with the scaling laws, verifying the effects of Pr, s and f_n, although there is a Pr effect on δ_{vi} which is not predicted by the scalings which thus need modifications to account for the complete Pr dependence.

ACKNOWLEDGMENTS

The support from the Australian Research Council is gratefully acknowledged.

CONFLICT OF INTERESTS

The authors declare that there are no conflict of interests.

ORCID

Wenxian Lin: http://orcid.org/0000-0001-5264-2097

S. W. Armfield: http://orcid.org/0000-0002-8032-0017

Mehdi Khatamifar: http://orcid.org/0000-0001-6273-7655

NOMENCLATURE

C_{vi}	ratio of the slope with Pr $\neq 10$ and the slope with Pr $= 10$ (dimensionless)
f	frequency of the sinusoidal heat flux (Hz)
f_n	$f/(V_c/L_c)$ (dimensionless)
g	gravitional acceleration (m/s^2), acting in the negative Y^* direction
L_c	characteristic length (m)
P	pressure (Pa)
Pr	Prandtl number, ν/α (dimensionless)
s	temperature stratification parameter, $\overline{T}_Y/T_X^0$ (dimensionless)
t	time (s)
t_{ht}	heating duration of the applied flux (s)
t_s	time scale attaining the QSS (s)
$t_{T,s}$	time scale for temperature boundary layer attaining the QSS (s)
$t_{vi,s}$	time scale for inner velocity boundary layer attaining the QSS (s)
T	temperature (^{o}C)
T_w	solid surface temperature (^{o}C)
$T_{w,s}$	solid surface temperature at t_s (^{o}C)
$T_X^0(t)$	temperature gradient across the solid surface at time t (^{o}C/m)
$\overline{T}$	ambient fluid temperature (^{o}C)
$\overline{T}_y$	ambient temperature gradient, $d\overline{T}/dY^*$ (^{o}C/m)
u, v	u^*/V_c, v^*/V_c (dimensionless)
u^*, v^*	horizontal and vertical velocities (m/s)
v_m	v_m^*/V_c (dimensionless)
$v_{m,s}$	$v_{m,s}^*/V_c$ (dimensionless)
$v_{m,T,s}$	v_m^* at $t_{T,s}$ (dimensionless)
v_m^*	maximum vertical velocity (m/s)
$v_{m,s}^*$	maximum vertical velocity at t_s (m/s)
V_c	characteristic velocity (m/s)
x, y	X^*/L_c, Y^*/L_c (dimensionless)
X^*, Y^*	horizontal and vertical coordinates (m)

GREEK SYMBOLS

α	thermal diffusivity (m^2/s)
β	thermal expansion coefficient (1/K)
δ_T	Δ_T/L_c (dimensionless)
$\delta_{T,s}$	$\Delta_{T,s}/L_c$ (dimensionless)
$\hat{\delta}_{T,s}$	scale for $\delta_{T,s}$ (dimensionless)
δ_{vi}	Δ_{vi}/L_c (dimensionless)
$\delta_{vi,s}$	$\Delta_{vi,s}/L_c$ (dimensionless)
$\hat{\delta}_{vi,s}$	scale for $\delta_{vi,s}$ (dimensionless)
Δ_T	temperature boundary-layer thickness (m)
$\Delta_{T,s}$	temperature boundary-layer thickness at t_s (m)
Δ_{vi}	inner velocity boundary-layer thickness
$\Delta_{vi,s}$	inner velocity boundary-layer thickness at t_s (m/s)
θ	$T/(\overline{\phi}_w L_c)$ (dimensionless)
θ_w	$T_w/(\overline{\phi}_w L_c)$ (dimensionless)
$\theta_{w,s}$	$T_{w,s}/(\overline{\phi}_w L_c)$ (dimensionless)
$\theta_{w,T,s}$	θ_w at $\tau_{T,s}$ (dimensionless)
ν	kinematic viscosity (m^2/s)
ρ	fluid density (kg/m^3)
τ	$t/(L_c/V_c)$ (dimensionless)
τ_{ht}	$t_{ht}/(L_c/V_c)$ (dimensionless)
τ_s	$t_s/(L_c/V_c)$ (dimensionless)
$\tau_{T,s}$	$t_{T,s}/(L_c/V_c)$ (dimensionless)
$\tau_{vi,s}$	$t_{vi,s}/(L_c/V_c)$ (dimensionless)
ϕ_w	constant heat flux across the solid surface ($^oC/m$)
$\overline{\phi}_w$	time-averaged value of $\phi_{wm}\sin(2\pi ft)$ ($^oC/m$)
ϕ_{wm}	maximum temperature gradient across the solid surface ($^oC/m$)

ABBREVIATIONS

BL	boundary layer
NCBL	natural convection boundary layer
QSS	quasi steady stage
SUS	start-up stage
TBL	temperature boundary layer
VBL	velocity boundary layer

References

[1] Duffie JA, Beckman WA. *Solar Engineering of Thermal Processes* (4th Edn). New York: John Wiley & Sons; 2013.

[2] Sergei K, Shen C, Jiang Y. A review of the current work potential of a trombe wall. Renew Sustain Energy Rev. 2020;130:109947.

[3] Fudholi A, Sopian K. A review of solar air flat plate collector for drying application. Renew Sustain Energy Rev. 2019;102:333-345.

[4] Khanal R, Lei C. A scaling investigation of the laminar convective flow in a solar chimney for natural ventilation. Int J Heat Fluid Flow. 2014;45:98-108.

[5] Monghasemi N, Vadiee A. A review of solar chimney integrated systems for space heating and cooling application. Renew Sustain Energy Rev. 2018;81:2714-2730.

[6] Faghri A, Zhang Y, Howell J. *Advanced Heat and Mass Transfer*. Columbia, MO: Global Digital Press; 2010.

[7] Lin W, Armfield SW, Patterson JC. Unsteady natural convection boundary-layer flow of a linearly-stratified fluid with $Pr \lesssim 1$ on an evenly heated semi-infinite vertical plate. Int J Heat Mass Transfer. 2008;51:327-343.

[8] Lin W, Armfield SW, Patterson JC, Lei C. Prandtl number scaling of unsteady natural convection boundary layers for Pr>1 fluids under isothermal heating. Phys Rev E. 2009;79:066313.

[9] Bednarz T, Lin, W, Patterson, JC, Lei, C, Armfield, SW. Scaling for unsteady thermo-magnetic convection boundary layer of paramagnetic fluids of $Pr > 1$ in micro-gravity conditions. Int J Heat Fluid Flow. 2009;30(6):1157-1170.

[10] Lin W, Armfield SW. Unified Prandtl number scaling for start-up and fully developed natural-convection boundary layers for both $Pr \gtrsim 1$ and $Pr \lesssim 1$ fluids with isothermal heating. Phys Rev E. 2012;86:066312.

[11] Lin W, Armfield SW. Scalings for unsteady natural convection boundary layers on an evenly heated plate with time-dependent heat flux. Phys Rev E. 2013;88:063013.

[12] Priam SS, Ikram MM, Saha S, Saha SC. Conjugate natural convection in a vertically divided square enclosure by a corrugated solid partition into air and water regions. Therm Sci Eng Prog. 2021;25:101036.

[13] Liu Y. Scaling of convective boundary layer flow induced by linear thermal forcing at $Pr < 1$ and $Pr > 1$. Phys Rev E. 2019;100:043112.

[14] Liu Y. Dynamics and scale analysis of the transient convective flow induced by cooling a $Pr < 1$ fluid with linear thermal forcing. Int J Heat Mass Transfer. 2020;154:119767.

[15] Bachiri M, Bouabdallah A. An analytic investigation of the steady-state natural convection boundary layer flow on a vertical plate for a wide range of Prandtl numbers. Heat Transfer Eng. 2010;31(7):608-616.

[16] Lin W, Armfield SW. Scalings for unsteady natural convection boundary layers on a vertical plate at time-dependent temperature. Int J Thermal Sci. 2017;111:78-99.

[17] Zhao Y, Zhao P, Liu Y, Xu Y, Torres JF. On the selection of perturbations for thermal boundary layer control. Phys Fluids. 2019;31:104102.

[18] Saha S, Brown R, Gu Y. Prandtl number scaling of the unsteady natural convection boundary layer adjacent to a vertical flat plate for $Pr > 1$ subject to ramp surface heat flux. Int J Heat Mass Transfer. 2012;55:7046-7055.

[19] Patterson JC, Imberger J. Unsteady natural convection in a rectangular cavity. J Fluid Mech. 1980;100:65-86.

[20] Bhowmick S, Xu F, Zhang X, Saha SC. Natural convection and heat transfer in a valley shaped cavity filled with initially stratified water. Int J Heat Mass Transfer. 2018;128:59-64.

[21] Liu Y, Bian Y, Zhao Y, Zhang S, Suo Q. Scaling laws for the transient convective flow in a differentially and linearly heated rectangular cavity at Pr $>$ 1. Phys Fluids. 2019;31:043601.

[22] Liu Y, Huang H. Effect of three modes of linear thermal forcing on convective flow and heat transfer in rectangular cavities. Int J Heat Mass Transfer. 2020;147:118951.

[23] Liu Y, Ren S. Scale law analysis of the curved boundary layer evolving around a horizontal cylinder at Pr $>$ 1. Phys Fluids. 2021;33:073614.

[24] Nie B, Xu F. Scales of natural convection on a convectively heated vertical wall. Phys Fluids. 2019;31:024107.

[25] Khatamifar M, Lin W, Dong L. Transient conjugate natural convection heat transfer in a differentially-heated square cavity with a partition of finite thickness and thermal conductivity. Case Studies Thermal Eng. 2021;25:100952.

[26] Bala NR, Bala SK, Saha LK, Hossain MA. Influence of undulating wall heat and mass flux on MHD natural convection boundary layer flow from a vertical wall. Heat Transfer. 2021;50:818–848

[27] Liu Y, Ren S. Improved scaling analysis of the transient buoyancy-driven flow induced by a linear temperature gradient. Int J Heat Mass Transfer. 2020;162:120386.

[28] Lin W, Armfield SW. Natural convection boundary-layer flow on an evenly heated vertical plate with time-varying heating flux in a stratified Pr $<$ 1 fluid. Numer Heat Transfer. A: Applications. 2019;76(6):393–419.

[29] Lin W, Armfield SW. Prandtl number scalings for unsteady natural convection boundary-layer flow on an evenly heated vertical plate in a homogeneous Pr $>$ 1 fluid. Numer Heat Transfer A: Applications. 2020;77(6):619–631.

[30] Lin W, Armfield SW, Khatamifar M. Scalings for unsteady natural convection boundary layer under time-varying heating flux in a small Prandtl number fluid. Case Studies Thermal Eng. 2021;27:101351.

[31] Zhou L, Armfield SW, Williamson N, Kirkpatrick MP, Lin W. Natural convection in a cavity with time-varying thermal forcing on a sidewall. Int J Heat Mass Transfer. 2020;150:119234.

[32] Loenko DS, Shenoy A, Sheremet MA. Effect of time-dependent wall temperature on natural convection of a non-Newtonian fluid in an enclosure. Int J Thermal Sci. 2021;166:106973.

[33] Hussam WK, Khanafer K, Salema HG, Sheard GI. Natural convection heat transfer utilizing nanofluid in a cavity with a periodic side-wall temperature in the presence of a magnetic field. Int Communi Heat Mass Transfer. 2019;104:127-135.

[34] Wu F, Wang G. Numerical simulation of natural convection in an inclined porous cavity under time-periodic boundary conditions with a partially active thermal side wall. RPC Adv. 2017;7:17519-17530.

[35] He W, Qin G, Wang Y, Bao Z. A segregated spectral element method for thermomagnetic convection of paramagnetic fluid in rectangular enclosures with sinusoidal temperature distribution on one side wall. Numer Heat Transfer A: Applications. 2019;76(2):51–72.

[36] Armfield SW, Patterson JC, Lin W. Scaling investigation of the natural convection boundary layers on an even heated plate. Int J Heat Mass Transfer. 2007;50:1592-1602.

[37] Wang W, Tian Z. Ding Y. Investigation on the influencing factors of energy consumption and thermal comfort for a passive solar house with water thermal storage wall. Energy Build. 2013;64:218-223.

[38] Hu Z, He W, Ji J, Zhang S. A review on the application of Trombe wall system in buildings. Renew Sustain Energy Rev. 2017;70:976-987.

[39] Hu Z, Zhang S, Hou J, He W, Liu X, Yu C, Zhu J. An experimental and numerical analysis of a novel water blind-Trombe wall system. Energy Convers Manag. 2020;205:112380.

[40] Mao Y, Lei C, Patterson, JC. Unsteady natural convection in a triangular enclosure induced by absorption of radiation – a revisit by improved scaling analysis. J Fluid Mech. 2009;622:75-102.

[41] Dittko KA, Kirkpatrick MP, Armfield SW. Three-dimensional simulation of natural convection in a reservoir sidearm. Phys Fluids 2013;25:025105.

[42] Mohamed MKA, Ong HR, Salleh MZ, Widodo B. Mixed convection boundary layer flow of engine oil nanofluid on a vertical flat plate with viscous dissipation. ASEAN J Automot. Technol. 2019;1:29-38.

[43] Younis O, Pallares J, Grau FX. Numerical study of transient laminar natural convection cooling of high Prandtl number fluids in a cubical cavity: Influence of the Prandtl number. World Acad Sci Eng Technol. 2007;36:116-121.

[44] Akbari A, Mohammadian E, Fazel SAA, Shanbedi M, Bahreini M, Heidari M, Dehkordi PB, Hussein SNCM. Natural convection from the outside surface of an inclined cylinder in pure liquids at low flux. ACS Omega 2019;4:7038-7046.

[45] Zhang T, Liu C, Gu Y, Jerome F. Glycerol in energy transportation: a state-of-the-art review. Green Chem. 2021;23:7865-7889.

[46] Lin W, Armfield SW. Unsteady natural convection on an evenly heated vertical plate for Prandtl number $Pr < 1$. Phys Rev E. 2005;72:066309.

[47] Kreith F, Manglik RM. *Principles of Heat Transfer* (8th Edn). Boston: Cengage Learning; 2016.

[48] Lin W, Armfield SW, Patterson JC. Cooling of a $Pr < 1$ fluid in a rectangular container. J Fluid Mech. 2007;574:85–108.